TU Delft

Delft University of Technology

Joint Inversion of Surface Wave Tomography and Body Wave Tomography Applied to 2D Media

Karimpour, M.; Slob, E.C.; Socco, LV

DOI
10.3997/2214-4609.202011637

Publication date
2020

Document Version
Final published version

Published in
82nd EAGE Conference & Exhibition 2020

Citation (APA)
Karimpour, M., Slob, E. C., & Socco, LV. (2020). Joint Inversion of Surface Wave Tomography and Body Wave Tomography Applied to 2D Media. In *82nd EAGE Conference & Exhibition 2020: 8-11 June 2020, Amsterdam, The Netherlands* (pp. 1-5). Article We_Dome5_05 EAGE. https://doi.org/10.3997/2214-4609.202011637

Important note
To cite this publication, please use the final published version (if applicable).
Please check the document version above.

Copyright
Other than for strictly personal use, it is not permitted to download, forward or distribute the text or part of it, without the consent of the author(s) and/or copyright holder(s), unless the work is under an open content license such as Creative Commons.

Takedown policy
Please contact us and provide details if you believe this document breaches copyrights.
We will remove access to the work immediately and investigate your claim.

This work is downloaded from Delft University of Technology.
For technical reasons the number of authors shown on this cover page is limited to a maximum of 10.

Green Open Access added to TU Delft Institutional Repository

'You share, we take care!' - Taverne project

https://www.openaccess.nl/en/you-share-we-take-care

Otherwise as indicated in the copyright section: the publisher is the copyright holder of this work and the author uses the Dutch legislation to make this work public.

2020 EAGE ANNUAL
82ND CONFERENCE + EXHIBITION
AMSTERDAM | THE NETHERLANDS
NOW IN WINTER
8-11 DECEMBER

We_Dome5_05

Joint Inversion of Surface Wave Tomography and Body Wave Tomography Applied to 2D Media

M. Karimpour[1,2]*, E. Slob[2], L.V. Socco[1]

[1] Politecnico Di Torino; [2] Delft University of Technology

Summary

Surface Wave Tomography is used to obtain a shear wave velocity model by inverting computed dispersion curves. Body Wave Tomography is used to obtain a longitudinal wave model through travel time inversion of picked first break travel times. Individual inversions suffer from various different limitations. Joint surface and body wave tomography inversion aims to reduce the limitations and produce better subsurface velocity models than either individual inversion. We integrate these two methods by inverting dispersion curves and first breaks simultaneously in a 2D joint inversion scheme. We propose a joint inversion algorithm in which Poisson's ratio provides the physical link between the shear and longitudinal wave velocities. The joint inversion results show encouraging improvements compared with individual inversion results.

Introduction

Seismic surface wave methods are usually performed to retrieve S-wave velocity models, and body wave tomography (BWT) is a tool which processes first arrival times to generate a subsurface P-wave velocity distribution. Regardless of the chosen seismic approach, inversion is a key step to build the subsurface velocity model. The inverse problem suffers from intrinsic limitation of each method: surface wave inversion is ill-posed and non-unique, while, BWT inversion in addition to being ill-posed and non-unique, usually fails to detect low velocity layers and too thin layers.

Joint inversion is a way to reduce the drawbacks of the inversion process of individual methods by inverting datasets from different methods simultaneously. The final model is hopefully a better representation of the subsurface than the individual inversion results. In other words, by applying a joint inversion scheme, the merits of different methods are put together to deliver a more reliable result. The different datasets can be related to each other by imposing structural constraints or physical links.

This work focuses on joint inversion of surface wave tomography (SWT) and BWT in 2D media, considering Poisson's ratio as the physical link between P- and S-wave velocities. Previous research has established that BWT and 1D surface wave analysis (SWA) can be used in a joint inversion scheme (Boiero and Socco., 2014). In SWA, the final model, which is a collection of 1D local models, might be laterally smoothed as a result of the moving windowing process which is applied during dispersion curve (DC) estimation. SWT is an alternative to the SWA method. Even though traditionally SWT has been applied in seismology, recently it has attracted considerable interest in near-surface applications such as mining exploration (Da Col et al., 2020). The ability of SWT to generate high resolution 2D or 3D S-wave velocity models makes it a tool of considerable interest. Using this feature, this study integrates BWT and SWT methods to obtain 2D velocity models.

In this work, P-wave and S-wave velocities are obtained using BWT and SWT methods, respectively. The main aim is to retrieve a subsurface model by joint inversion of BWT and SWT data and compare the results with results from individual inversions.

In the following, firstly the applied method is illustrated. Then, the results of joint inversion of BWT and SWT are shown and compared with individual inversion results. Finally, the impact of applying a physical link on the joint inversion results is depicted.

Method

The input for BWT are the travel times picked for each source-receiver couple in the dataset. The input for SWT are the average slowness dispersion for each receiver pair in line with a source. The average slowness dispersion curves are estimated using a modified two-station method (see Da Col et al., 2020, for details).
The input parameter for the forward model are the density, P-wave, and S-wave velocities of each layer. Due to low sensitivity of the methods to the density values, they are assumed to be known as a priori information.
The final model is calculated by minimizing the following misfit function (Q), as proposed by Boiero and Socco (2014):

$$Q = \left[\left(\mathbf{d}_{\mathbf{obs}} - fw(\mathbf{m})\right)^T \mathbf{C}_{\mathbf{obs}}^{-1}\left(\mathbf{d}_{\mathbf{obs}} - fw(\mathbf{m})\right)\right] + \left[\left(\mathbf{m}_{\mathbf{prior}} - \mathbf{m}\right)^T \mathbf{C}_{\mathbf{prior}}^{-1}\left(\mathbf{m}_{\mathbf{prior}} - \mathbf{m}\right)\right]$$
$$+ \left[\left(-\mathbf{Rm}\right)^T \mathbf{C}_{\mathbf{R}}^{-1}\left(-\mathbf{Rm}\right)\right] + \left[\left(\mathbf{pr} - pr(\mathbf{m})\right)^T \mathbf{C}_{\mathbf{pr}}^{-1}\left(\mathbf{pr} - pr(\mathbf{m})\right)\right] \qquad (1)$$

Where $\mathbf{d}_{\mathbf{obs}}$ and $\mathbf{C}_{\mathbf{obs}}$ are the input data and the corresponding covariance matrix, fw denotes the forward response of the model, $\mathbf{m}_{\mathbf{prior}}$ represents the initial model and $\mathbf{C}_{\mathbf{prior}}$ is the covariance matrix of the initial model, $\mathbf{R}$ represents the spatial regularization matrix (proposed by Auken and Christiansen (2004)) and

$\mathbf{C_R}$ represents its covariance matrix. Having the physical link indicates minimizing Poisson's ratio of the model *pr*(**m**) with respect to an expected value **pr,** and $\mathbf{C_{pr}}$ is the corresponding covariance matrix. A quasi-Newton damped least squares algorithm (Tarantola, 1987) is applied to minimize the misfit function of eq. (1). Therefore, the updated model ($\mathbf{m_{n+1}}$) at the nth iteration is computed as:

$$\mathbf{m}_{n+1} = \mathbf{m}_n + \left(\begin{bmatrix} \mathbf{G}_J^T \mathbf{C}_{obs}^{-1} \mathbf{G}_J + \mathbf{P}^T \mathbf{C}_{prior}^{-1} \mathbf{P} + \mathbf{R}^T \mathbf{C}_R^{-1} \mathbf{R} + \mathbf{G}_{pr}^T \mathbf{C}_{pr}^{-1} \mathbf{G}_{pr} + \lambda \mathbf{I} \end{bmatrix}^{-1} \times \begin{bmatrix} \mathbf{G}_J^T \mathbf{C}_{obs}^{-1} \left(\mathbf{d}_{obs} - fw(\mathbf{m}_n) \right) + \mathbf{P}^T \mathbf{C}_{prior}^{-1} \left(\mathbf{m}_{prior} - \mathbf{m}_n \right) \\ + \mathbf{R}^T \mathbf{C}_R^{-1} \left(-\mathbf{R}\mathbf{m}_n \right) + \mathbf{G}_{pr}^T \mathbf{C}_{pr}^{-1} \left(\mathbf{pr} - pr(\mathbf{m}) \right) \end{bmatrix} \right) \quad (2)$$

Where $\mathbf{G_J}$ is the sensitivity matrix of the data, **P** is a matrix that contains the partial derivative values of the initial model with respect to the unknowns, $\mathbf{G_{pr}}$ represents the partial derivatives of the physical link with respect to the unknowns, λ stands for the damping factor (for details see Marquardt, 1963).

Synthetic Example

The synthetic datasets have been generated using a finite difference code (see Qin et al., 2019, for details). The model presents a vertical uplift in the bottom-right part of the model. The source emits a 20 Hz Ricker wavelet. The receivers are located every metre along the line and there are 25 shots with 5 m spacing. The seismic properties of the model are presented in Table 1. The geometry and P- and S-wave velocity values in the model are shown in Figures 1a and 1b, respectively. The seismic properties of the initial model that was used in the inversion scheme are presented in Table 2.

As mentioned earlier, several receiver couples are needed to extract a dispersion curve in the tomographic approach. Here, the chosen minimum receiver separation was 4 m, and the maximum separation was set to 30 m. Then, the modified two-station method (Da Col et al., 2020) was applied on each receiver couple to get the dispersion information. For each receiver couple, the obtained cross-multiplication matrices from different shots were stacked to increase the signal to noise ratio. Repeating this procedure for different receiver pairs, 664 dispersion curves were retrieved (Figure 1c).

These extracted dispersion curves and first breaks (Figure 1d) were inverted using eq. (2) and the results were compared with individual inversions in Figure 2.

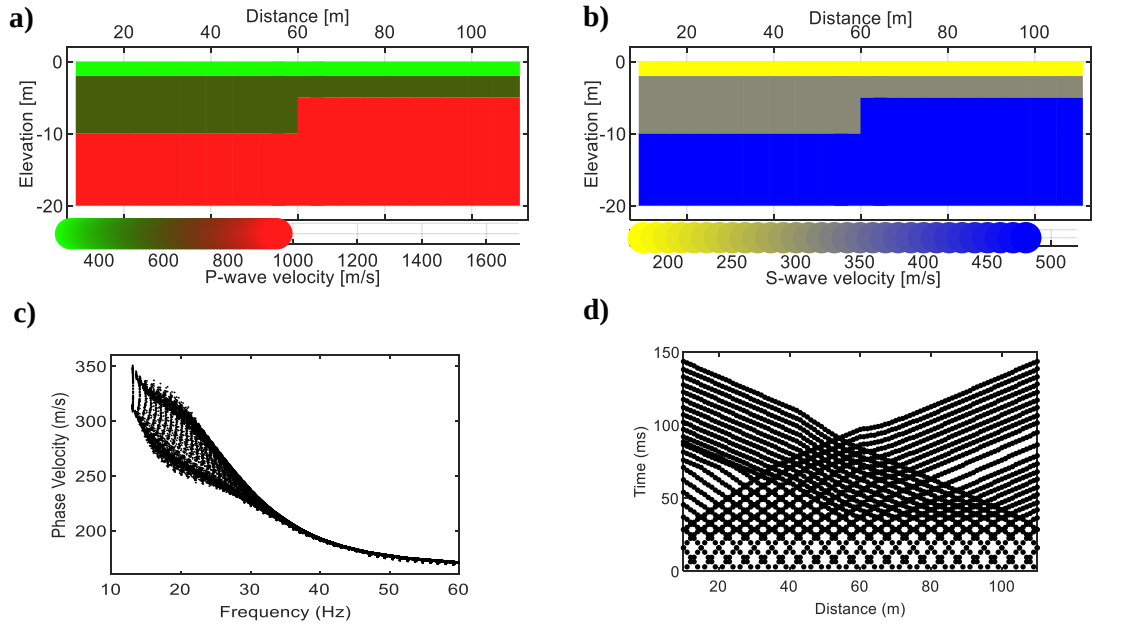

Figure 1 a) *P-wave velocity of the model b) S-wave velocity of the model c) All retrieved dispersion curves c) First break travel times as a function of distance*

Table 1 *Geophysical parameters of the Model*

Layer	V_S (m/s)	V_P (m/s)	h (m)	ρ (g/cm^3)
1	180	310	2	2
2	320	590	3-8	2.1
3	480	950	-	2.2

Table 2 *Geophysical parameters of the initial model*

Layer	V_S (m/s)	V_P (m/s)	h (m)	ρ (g/cm^3)
1	200	300	3	2
2	300	600	6	2.1
3	500	930	-	2.2

In our 2D inversion scheme, it is necessary to define the width each grid point and the number of layers. The width of each grid point was set to 6 m and 2 layers were defined above the half-space. Poisson's ratio was considered as the physical link between S-wave and P-wave velocities. In the update of the damping factor at each iteration, the Poisson's ratio of the model is evaluated as well. If the values of Poisson's ratio are not physical (not in the range of 0-0.5), the damping factor is changed and the new model $\mathbf{m}_{n+1}$ is computed again using eq. (2). This process continues until the new model contains physical values of Poisson's ratio.

The inversion process updates the initial model according to eq. (2). The joint inversion and individual inversion results, after 15 iterations, are depicted in Figure 2.

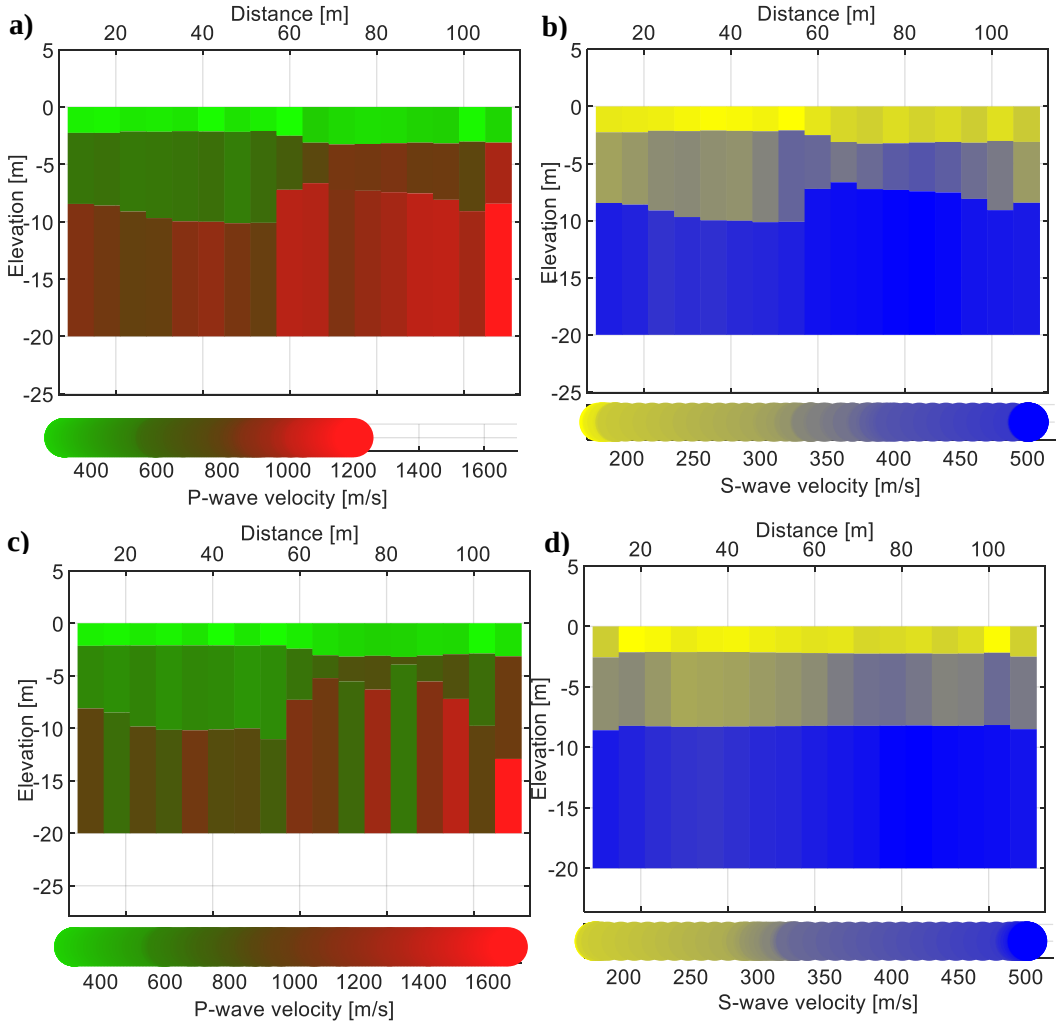

Figure 2 *The inversion results a) P-wave velocity model of joint inversion b) S-wave velocity model of joint inversion c) P-wave velocity model resulting from individual BWT inversion d) S-wave velocity model acquired from individual SWT inversion.*

The joint inversion scheme has generated velocity models which are closer to the true model. In case of

individual BWT inversion (Figure 2c), the lateral oscillation of the velocity in the third layer is considerable with a maximum velocity value of more than 1600 m/s which is far from the true velocity of the third layer (950 m/s). This oscillation has reduced significantly by applying the joint inversion algorithm (Figure 2a). Figure 2c shows that the thickness of the second layer in locations where the position is more than 60 m, cannot be resolved properly by individual BWT inversion since this layer is too thin and acts as a hidden layer. This is most severe for the positions at the range of 84-90 m where the obtained thickness of the second layer is less than 0.5 m. However, applying the joint inversion scheme reduced this problem (Figures 2a and 2b).
Moreover, the improved S-wave velocity model obtained by joint inversion compared with the single inversion result is clear. Even though the individual SWT inversion successfully found the interface between the first and the second layers, it fails to locate the second interface correctly. However, the joint algorithm can find this interface more accurately. Joint inversion produces a better model than individual inversions in both interface location and layer velocity values.

Conclusions

Joint inversion of BWT and SWT can produce more reliable P-wave and S-wave velocity models than individual inversions. From comparing joint inversion results and the individual inversion results we conclude that the proposed joint inversion scheme produces better subsurface velocity models. Interfaces and layer velocities are better with joint inversion than with individual inversions. Having a physical link between the inversion parameters can further increase the accuracy of the joint inversion results. We observe that in our single model study joint inversion deals with issues like resolving a thin layer better than individual inversions. This is possibly an indication that joint inversion decreases the solution space and thereby reduces the risk of falling into a local minimum.

Acknowledgements

The PhD scholarship of Mohammadkarim Karimpour is funded by Compagnia di San Paolo in the framework of the Joint Project Program. The authors thank Shufan Hu for providing the synthetic data.

References

Auken, E., and A. V. Christiansen, [2004], Layered and laterally constrained 2D inversion of resistivity data: *Geophysics*, 69, 752–761, DOI: 10.1190/1.1759461.

Da Col, F., Papadopoulou, M., Koivisto, E., Sito, L., Savolainen, M., and L. V. Socco, [2020], Application of surface-wave tomography to mineral exploration: a case study from Siilinjärvi, Finland: *Geophysical Prospecting*, 2020, 68, 254-269, DOI: 10.1111/1365-2478.12903.

Boiero, D., and L. V. Socco, [2014], Joint inversion of Rayleigh-wave dispersion and P-wave refraction data for laterally varying models*: Geophysics, 79*, no. 4, EN49–EN59, DOI: 10.1190/geo2013-0212.1.

Marquardt, D. W., [1963], An algorithm for least squares estimation of nonlinear parameters: *Journal of the Society of Industrial Applied Mathematics, 11,* 431–441, DOI: 10.1137/0111030.

Qin, T., Zhao, Y., Hu, S., An, C., Bi, W., Ge, S., Capineri, L., and T. Bohlen, [2019] An interactive integrated interpretation of GPR and Rayleigh Wave Data Based on the Genetic Algorithm. *Surveys in Geophysics*, 1-26, DOI: 10.1007/s10712-019-09543-x

Tarantola, A., 1987, Inverse problem theory: Methods for fata fitting and model parameter estimation: *Elsevier Science.*